

# Determining the Effect of Concrete Roadways on Gamma-ray Background for Radiation Portal Monitoring Systems

**Christopher M. Ryan<sup>1</sup>, Craig M. Marianno<sup>1</sup>, William S. Charlton<sup>1</sup>,  
Alexander A. Solodov<sup>2</sup>, Ronald J. Livesay<sup>2</sup>**

<sup>1</sup>Nuclear Security Science and Policy Institute, Texas A&M University,  
College Station, Texas 77843-3473 USA

<sup>2</sup>Global Nuclear Security Technology Division, Oak Ridge National Laboratory,  
Oak Ridge, Tennessee 37831-6010 USA

## **Abstract:**

*The dissolution of the Soviet Union coupled with the growing sophistication of international terror organizations has brought about a desire to ensure that a sound infrastructure exists to interdict smuggled nuclear material prior to it leaving its country of origin. To combat the threat of nuclear trafficking, radiation portal monitors (RPMs) are deployed around the world to intercept illicit material while in transit by passively detecting gamma and neutron radiation. Portal monitors in some locations have reported abnormally high background counts with little or no consistency. The higher background data has been attributed, in part, to the concrete surrounding the portal monitors. Higher background increases the minimum detectable activity and can ultimately lead to more material passing through the RPMs undetected.*

*This work was focused on understanding the influence of the concrete surrounding the monitors on the total gamma-ray background for the system. The study combined destructive and nondestructive analytical techniques with computer simulations to form a quantitative model that is adaptable to any RPM configuration. Six samples were taken from three different composition concrete slabs. The natural radiological background of these samples was determined using a high-purity germanium (HPGe) detector in conjunction with the Canberra In-Situ Object Counting System (ISOCS™) and Genie™ 2000 software packages. The composition of each sample was determined using neutron activation analysis (NAA) techniques. The results from these experiments were incorporated into a Monte Carlo N-Particle (MCNP) photon transport simulation to determine the number of gamma-rays from the different concrete slabs detected by the RPM.*

**Keywords:** smuggling; trafficking; NAA; RPM; concrete

## **1. Introduction**

The collapse of the Soviet Union in 1991 ushered in an era of uncertainty concerning the security of the radiological and nuclear material holdings of the Russian Federation along with the other countries of the Former Soviet Union (FSU). In addition, the 11 September 2001 terrorist attacks on the United States highlighted the growing sophistication of international terrorist organizations, along with their desire to inflict mass civilian casualties. The combination of possibly unsecured radiological and nuclear material, porous borders throughout the FSU, and terrorist organizations seeking to acquire such material,

makes radiation detection and ports of entry (POEs) a vital step in combating nuclear smuggling.

From 1991-2006, more than 40% of reported illicit nuclear material trafficking cases had a nexus in Russia and the FSU [1]. To reduce this threat, the United States Government (USG) has engaged in multiple partnerships to provide radiation detection material – including radiation portal monitors (RPMs) – for use at POEs to intercept smuggled radiological or nuclear materials.

RPMs are designed for vehicular, rail, or pedestrian traffic, but in each case they are

used to passively detect gamma and/or neutron radiation. Gammas are detected in the RPMs using any number of different detector technologies; however, this research was specifically focused on gamma detection in vehicular RPMs using polyvinyl toluene (PVT) scintillators. The methods described in this paper may be adapted for any RPM configuration.

When not occupied by a vehicle, RPMs continuously measure the background radiation in the surrounding areas and adjust the alarm thresholds accordingly. In some locations, the RPMs reported abnormally high gamma-ray background with little or no consistency. It is possible that the natural occurring radiological material (NORM) in the concrete roadways beneath the RPMs is contributing to this anomalous data. Higher background levels will increase the minimum detectable activity (MDA) of the RPMs, thereby raising the threshold for radiation alarms and increasing the probability of illicit radiological or nuclear materials passing through the portals undetected. A picture of the RPM modeled for this research is shown in Figure 1.



**Figure 1:** The RPM modeled for this research.

## 2. Experiments and simulations

The primary objective of this research was to develop a method for determining the natural radiological background and elemental composition of the concrete underneath and around an RPM in order to estimate its contribution to the overall gamma-ray background. This method was developed using a combination of established analytical techniques and photon transport simulations.

### 2.1. Gamma-ray background measurements

Six core-drilled concrete cylinders from three different composition concrete slabs were acquired from Oak Ridge National Laboratory (ORNL) for use during this research. The samples were labeled for identification. Samples from the same slab are identified with the same letter. The dimensions and masses of each sample were measured in order to calculate the density of the concrete. A picture of the concrete samples is shown in Figure 2.



**Figure 2:** The concrete samples used for this research.

Gamma spectra were collected for each sample using an HPGe semiconductor detector, the Genie™ 2000 spectroscopy software, and a multichannel analyzer (MCA). A lead vault was constructed around the detector to prevent interference from the concrete walls of the laboratory and radioactive check sources in the room. Prior to measuring any samples, a 24 h background spectrum was taken for later reference. After acquiring a background spectrum, a sample was placed in the vault and a 24 h spectrum was collected. This was repeated for the remaining samples. A picture of the detector geometry is given in Figure 3.

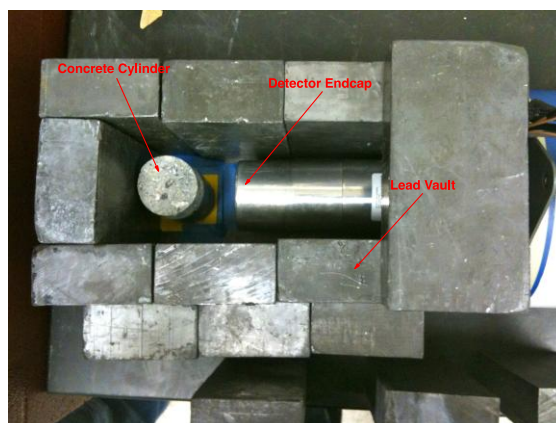


**Figure 3:** A picture of the detector geometry used for the concrete background measurements.

## 2.2. Neutron activation analysis

A combination of thermal and fast neutron activation analysis (NAA) was conducted to determine the elemental composition of the concrete samples. Prior to any analysis, gram-sized portions of each sample were broken off and ground into a powder. The powder was placed into polyethylene vials for irradiation. Additionally, each measurement involved the use of one or more comparator standards and quality control materials.

The neutron source for the thermal NAA irradiations was a 1 MW TRIGA research reactor located at the Texas A&M University Nuclear Science Center (NSC). The thermal neutron flux in the reactor was  $10^{13} \text{ cm}^{-2} \text{ s}^{-1}$  during the experiments. For the first irradiation, the sample, standard, and quality control vials were sent into the core, irradiated for 30 s, returned, and allowed to decay for 1200 s. The sample vial was then placed on an HPGe detector and counted in live-time for 500 s. For the second irradiation, the vials were placed into an aluminum canister. The canister was sealed and irradiated in the reactor for 14 h. Afterwards, the vials were removed from the canister and allowed to decay for approximately six days, after which they were counted in live-time for 2000 s on an HPGe detector. After counting, the vials were placed aside and allowed to decay for an additional 20 days. Following the second decay period, the vials were counted in live-time for 10 800 s on the same HPGe detector.

The neutron source for the fast NAA irradiations was a Kaman Sciences Corporation A-711 sealed-tube neutron generator located at the Texas A&M University Center for Chemical Characterization and Analysis (CCCA). The A-711 generates 14.8 MeV fast neutrons through the  ${}^3\text{H}({}^2\text{H},n){}^4\text{He}$  fusion reaction. The beam intensity of the generator was between  $10^9$  and  $10^{10} \text{ s}^{-1}$  during the measurements. The fast NAA measurements were used to determine the oxygen and silicon concentrations of the concrete. For the silicon measurements, the sample vials were sent to the generator, irradiated for 300 s, and returned. The samples decayed for approximately 60 s during transport to an HPGe detector where they were counted in live-time for 300 s. For the oxygen measurements, the samples were sent to the generator and irradiated for 20 s, then they were returned and counted on two summed NaI(Tl) detectors placed at  $180^\circ$ . The detectors were discriminated against any

signals below 4500 keV. This method of oxygen determination with fast NAA was previously described by W. Ehmann and W. James [2,3].

## 2.3. Determination of concrete composition

The concentrations of multiple elements in the samples were determined using the relative method, which is given by:

$$\omega = \omega^* \frac{m^* A}{mA^*} \quad (1)$$

where  $\omega$  is the concentration of the desired element,  $m$  is the mass of the sample,  $A$  is the decay-corrected activity of the sample, and the "\*" superscript denotes the comparator standard [4]. The concentrations of carbon and hydrogen cannot be determined through thermal or fast NAA techniques; therefore, the concentrations of both elements were estimated for each sample based on the total weight percentage of the samples determined by the measurements. The total weight percentage of elements characterized through NAA for each sample was also determined by summing the individual concentrations.

## 2.4. Generation of efficiency calibration files with ISOCS™

After determining the composition of each sample, efficiency calibration files were generated using the ISOCS™ software. The measured dimensions and calculated densities were input into a vendor-supplied cylinder template. The NAA results were used to define a custom material for each concrete sample. A series of mathematical algorithms describing the response characteristics of the detector as a function of energy, angle, and distance from the detector was generated by the software for use with Genie™ 2000.

## 2.5. Determination of concrete background activity

Once the efficiency calibration files were generated, the background activities of the isotopes present in each concrete sample were calculated using the Genie™ 2000 software. The ISOCS™ calibration files were applied to each spectrum from the concrete samples. Gamma-ray energy peaks were located and their areas determined using the built-in algorithms available in the software package. The 24 h background spectrum was subtracted

from each sample spectrum, and nuclide identification was conducted using a customized nuclide library definition. The software was then used to calculate a specific activity for each of the gamma-ray energies found in the spectrum, and then compute a weighted mean specific activity for each identified isotope.

## 2.6. Generation of radioactive source terms for MCNP simulations

The background activity calculations were used to generate a source term for each sample that was used to define a distributed radioactive source throughout the concrete slab. The emission probabilities for the identified gamma-ray peak energies in each slab were calculated as follows:

$$P_E^i = \frac{A^i y_E^i}{\sum_{i=1}^N A^i y_E^i} \quad (2)$$

where  $P_E^i$  is the emission probability of a gamma-ray with energy,  $E$  for an isotope,  $i$ ,  $A^i$  is the total activity of isotope,  $i$  in the slab,  $y_E^i$  is the yield of a gamma-ray with energy,  $E$ , indicative of isotope,  $i$ , and  $N$  is the total number of identified isotopes in the sample.

## 2.7. MCNP simulations

The photon transport simulations were completed using the Monte Carlo N-Particle (MCNP) version 5 transport code [5]. A model of the physical RPM was constructed in MCNP and separate input files were saved for each sample. For each input deck, the NAA results were used to define the material composition of the concrete in the model. The radioactive source term calculations were used to create a distributed radioactive source throughout the volume of each concrete slab. An image of the RPM model is shown in Figure 4.

In order to determine count rates in the RPM, F8 pulse height tallies were applied to each PVT detector volume and the result was multiplied by the total gamma-ray emission rate for the concrete slab. Comparisons were then made between the count rate predicted by MCNP and the actual count rate recorded by the RPM in the presence of one of the concrete slabs. The model was validated by comparing the actual and predicted count rates for the RPM in the presence of varying-strength  $^{137}\text{Cs}$  check sources.

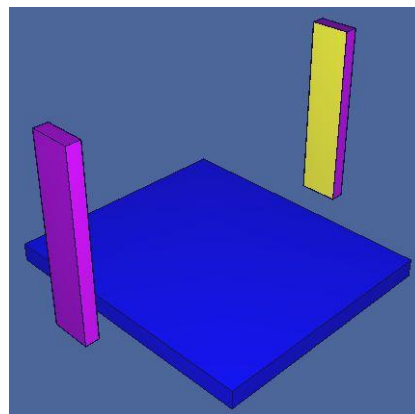


**Figure 4:** An image of the RPM modeled using the MCNP transport code.

Two sensitivity analyses were conducted to verify calculations and assumptions critical to the model. For the first analysis, the model was rerun with the concrete density set to  $\pm 2\sigma$  to determine the impact of large density fluctuations on the results. Since the carbon and hydrogen concentrations could not be determined with the NAA techniques employed, the second analysis focused on determining the impact of major fluctuations in their concentrations from an assumed value. Each deck was rerun with the carbon content set to 50% and 10% of this assumed value. The difference in the new total weight percentage and 100% was filled with hydrogen to prevent MCNP from renormalizing the weight fractions of the other elements in the slab.

## 3. Results and Discussion

### 3.1. Elemental composition of concrete samples

The concentrations of select elements in the quality control samples are given in Table 1 along with their associated literature values. The results show that for major constituent elements the quality control samples were within  $\pm 2\sigma$  of their stated literature values. Not only did this serve as validation of the comparator standards, but showed that the results for the concrete samples were both precise and accurate. The uranium and thorium concentrations of each concrete sample are given in Table 2. The results show a statistically significant difference in the uranium and thorium concentrations of samples G1 and G2 and the thorium concentrations of samples L1 and L2.

Element	Concentration $\pm \sigma$	
	Quality Control	Literature [6]
Al	9.17 $\pm$ 0.12 %	9.18 $\pm$ 0.05 %
Fe	7.10 $\pm$ 0.01 %	7.21 $\pm$ 0.08 %
K	Below Limits	0.16 $\pm$ 0.01 %
Mg	1.18 $\pm$ 0.06 %	Below Limits
Mn	0.13 $\pm$ 0.01 %	0.12 $\pm$ 0.01 %
Na	1.53 $\pm$ 0.01 %	1.59 $\pm$ 0.03 %
O	30.77 $\pm$ 3.04 %	31.34 %
Si	28.35 $\pm$ 0.11 %	27.67 $\pm$ 0.27 %
Th	Below Limits	282 $\pm$ 19 ppb
Ti	0.77 $\pm$ 0.03 %	0.71 $\pm$ 0.02 %
U	Below Limits	320 $\pm$ 180 ppb

**Table 1:** Concentrations of select elements for quality control samples and their associated literature values.

Sample	Concentration $\pm \sigma$ (ppm)	
	U	Th
F1	1.16 $\pm$ 0.11	0.71 $\pm$ 0.22
F2	1.15 $\pm$ 0.07	0.94 $\pm$ 0.18
G1	2.75 $\pm$ 0.20	10.02 $\pm$ 0.05
G2	4.63 $\pm$ 0.32	14.26 $\pm$ 0.09
L1	1.54 $\pm$ 0.08	1.89 $\pm$ 0.02
L2	1.35 $\pm$ 0.09	2.25 $\pm$ 0.03

**Table 2:** Concentrations of uranium and thorium in different concrete samples.

### 3.2. Background activity of concrete samples

The specific activities of background isotopes in the concrete samples in given in Table 3. It should be noted that the  $^{226}\text{Ra}$  and  $^{232}\text{Th}$  isotopes are assumed to be in secular equilibrium with their respective daughter products. The  $^{234}\text{Th}$  isotope – while the parent nuclide of  $^{226}\text{Ra}$  – has been reported independently of the decay chain in order to validate this assumption.

Generally, between samples from the same slab, the specific activities of the identified isotopes are within  $\pm 2\sigma$  of each other. One exception to this is the  $^{234}\text{Th}$  activity in samples from slab G. The calculated  $^{234}\text{Th}$  activity in sample G2 is approximately 44% larger than the activity calculated for sample G1. From Table 3, the uranium and thorium concentrations of sample G2 are approximately 41% and 30% greater, respectively, than those of sample G1. Also, the specific activity of the  $^{232}\text{Th}$  parent nuclide is approximately 7% larger in sample G1, indicating that although sample G2 has a greater overall concentration of thorium,

sample G1 contains more of the naturally occurring  $^{232}\text{Th}$  isotope. Since sample G1 contains a greater amount of  $^{232}\text{Th}$ , and natural uranium is composed primarily of the  $^{234}\text{Th}$  parent nuclide,  $^{238}\text{U}$ , the greater specific activity of  $^{234}\text{Th}$  in sample G2 is a result of the larger overall uranium content of the sample.

Sample	Specific Activity $\pm \sigma$ (Bq kg $^{-1}$ )			
	$^{40}\text{K}$	$^{226}\text{Ra}$	$^{232}\text{Th}$	$^{234}\text{Th}$
F1	42.27 $\pm$ 4.69	10.67 $\pm$ 0.50	4.97 $\pm$ 0.37	12.74 $\pm$ 2.28
F2	36.58 $\pm$ 4.63	10.55 $\pm$ 0.52	4.65 $\pm$ 0.38	13.34 $\pm$ 2.33
G1	696 $\pm$ 30	64.34 $\pm$ 1.84	80.21 $\pm$ 1.56	48.21 $\pm$ 5.15
G2	735 $\pm$ 32	67.70 $\pm$ 2.05	74.56 $\pm$ 1.56	85.56 $\pm$ 9.17
L1	170 $\pm$ 9	13.08 $\pm$ 0.61	9.58 $\pm$ 0.53	15.47 $\pm$ 2.50
L2	151 $\pm$ 8	12.70 $\pm$ 0.62	7.87 $\pm$ 0.46	18.43 $\pm$ 2.68

**Table 3:** Specific activities of background isotopes identified in different concrete samples.

### 3.3. Contribution of concrete to gamma-ray background

The average count rate per detector predicted by MCNP for each concrete sample is given in Table 4. Please note for this paper that the quoted uncertainties for MCNP results are only indicative of the MCNP statistical uncertainty.

Sample	Average Count Rate $\pm \sigma$ (counts s $^{-1}$ detector $^{-1}$ )	
	0.0 – 3.0 MeV	40 – 140 keV
F1	84.29 $\pm$ 0.60	11.17 $\pm$ 0.22
F2	80.08 $\pm$ 0.58	10.71 $\pm$ 0.21
G1	950 $\pm$ 6	120 $\pm$ 2
G2	951 $\pm$ 6	120 $\pm$ 2
L1	164 $\pm$ 1	19.92 $\pm$ 0.39
L2	146 $\pm$ 1	17.83 $\pm$ 0.35

**Table 4:** The average detector count rate in the RPM predicted by MCNP.

The count rates determined by MCNP are consistent with the results from the specific activity measurements. Slab G had the highest total activity, followed by slabs L and F. It is expected that the larger activity would lead to a higher count rate in the RPM. It is worth noting that sample L1 has a count rate approximately 10% higher than that of sample

L2. The results given in Table 3 show that sample L1 has a total activity approximately 9% higher than that of sample L2. The higher total activity for sample L1 indicates that more gammas will be emitted from the slab and subsequently detected by the RPM.

A comparison of actual and estimated count rates from the RPM to the predicted values from MCNP for slab G is given in Table 5. The actual count rates for each detector were obtained by taking a 24 h average from a RPM data printout. It should be noted that the actual count rates from the RPM could also include counts derived from environmental background or electronic noise. These extraneous signals make it difficult to determine the validity of the MCNP model, which only considers gamma-rays generated from the concrete slab. A 12 h average was taken from a RPM data printout for a time period where no concrete slab was present. This was subtracted from the actual count rates to obtain the estimated count rates.

Data Set	Count Rate $\pm \sigma$ (counts s <sup>-1</sup> )			
	Left, Upper	Left, Lower	Right, Upper	Right, Lower
RPM (Actual)	273 $\pm 17$	315 $\pm 18$	290 $\pm 17$	338 $\pm 18$
RPM (Estimated)	90 $\pm 10$	144 $\pm 12$	99 $\pm 10$	161 $\pm 13$
G1 (MCNP)	101 $\pm 2$	137 $\pm 2$	104 $\pm 2$	137 $\pm 2$
G2 (MCNP)	103 $\pm 2$	140 $\pm 2$	105 $\pm 2$	134 $\pm 2$

**Table 5:** A comparison of different RPM detector count rates for slab G.

In each case, the count rates in the upper detectors are less than those in the lower detectors. This is expected because the lower detectors are closer to the concrete slab, and therefore closer to the source of the gamma-rays. The data also shows that the MCNP results are consistent between samples G1 and G2. This is important to note because the larger amount of uranium and thorium in sample G2 did not impact the overall count rate. Since the highest yield gamma-rays from the decay of <sup>234</sup>Th are 63 and 93 keV, it is possible that they do not reach any of the PVT scintillators due to attenuation in the slab, the surrounding air, or the RPM structural material.

The data in Table 5 shows that it is possible to obtain a reasonable estimate of the gamma-ray contribution from the concrete using

MCNP. Even though the estimated RPM count rates were within  $\pm 2\sigma$  of the MCNP results, there are a few sources of error that could impact the results. It was assumed that the lower level discriminator on the physical RPM was set between 40 and 140 keV. The count rates in the RPM could be higher or lower if incorrect discrimination settings were applied. Additionally, subtracting the 12 h averaged data from a different 24 h data set could also impact the results. Since environmental background can vary based on any number of external factors, the estimated RPM count rate may not be an accurate representation of the count rate from only the concrete.

### 3.4. Model validation and sensitivity analysis

The MCNP model was tested by measuring the response of the RPM to different strength <sup>137</sup>Cs check sources and comparing the count rates to those predicted by the code. A comparison of the RPM and MCNP count rates is given in Table 6. A ratio of the MCNP and RPM results was also calculated to identify and potential bias in the MCNP results. This ratio is also given in Table 6.

Source Strength (μCi)	Count Rate $\pm \sigma$ (counts s <sup>-1</sup> )		MCNP RPM <sup>-1</sup> $\pm \sigma$
	RPM	MCNP	
5	18.75 $\pm 4.33$	13.38 $\pm 0.14$	0.71 $\pm 0.16$
10	35.00 $\pm 5.92$	26.77 $\pm 0.29$	0.77 $\pm 0.13$
15	50.60 $\pm 7.11$	40.15 $\pm 0.43$	0.79 $\pm 0.11$
20	68.85 $\pm 8.30$	53.53 $\pm 0.58$	0.78 $\pm 0.09$

**Table 6:** A comparison of RPM and MCNP count rates for various <sup>137</sup>Cs check sources.

The data in Table 6 shows that the count rate in the physical detector exceeded the count rate simulated in the MCNP model; however, the ratio of the simulated and measured data is statistically the same for all measurements. This validation case indicates that there is a certain amount of bias to the MCNP model. The RPM value was – on average – approximately 24% larger than the value predicted by MCNP. This difference could be caused by electronic noise introducing extraneous counts into the system. It is also possible that the energy window settings on the RPM drifted during the measurements,

causing an inconsistency with the MCNP simulations. Additionally, the MCNP model also does not incorporate the light collection efficiencies of the PVT scintillators or their photomultiplier tubes (PMTs).

Two sensitivity analyses were completed to verify measurements and assumptions in this research. Each MCNP deck was rerun with the concrete density set to  $\pm 2\sigma$  of the calculated value. A comparison of the average count rates is given in Table 7. Additionally, the MCNP decks were rerun with the carbon content set to 50% and 10% of the assumed value. A comparison of these results is given in Table 8. A carbon content sensitivity analysis was not completed for sample G2 because the elemental concentrations determined through NAA had already accounted for the entire weight percentage of the sample.

Sample	Average Count Rate $\pm \sigma$ (counts s <sup>-1</sup> detector <sup>-1</sup> )		
	-2 $\sigma$	Calculated	+2 $\sigma$
F1	11.26 $\pm 0.22$	11.17 $\pm 0.22$	11.14 $\pm 0.22$
F2	10.76 $\pm 0.21$	10.71 $\pm 0.21$	10.63 $\pm 0.21$
G1	121 $\pm 2$	120 $\pm 2$	120 $\pm 2$
G2	121 $\pm 2$	120 $\pm 2$	120 $\pm 2$
L1	20.03 $\pm 0.39$	19.92 $\pm 0.39$	19.80 $\pm 0.39$
L2	17.97 $\pm 0.35$	17.83 $\pm 0.35$	17.76 $\pm 0.35$

**Table 7:** A comparison of count rates for different concrete samples with varying densities.

Sample	Average Count Rate $\pm \sigma$ (counts s <sup>-1</sup> detector <sup>-1</sup> )		
	Assumed	50%	10%
F1	11.17 $\pm 0.22$	10.82 $\pm 0.22$	10.21 $\pm 0.21$
F2	10.71 $\pm 0.21$	10.44 $\pm 0.21$	9.96 $\pm 0.21$
G1	120 $\pm 2$	119 $\pm 2$	118 $\pm 2$
L1	19.92 $\pm 0.39$	19.53 $\pm 0.39$	18.58 $\pm 0.38$
L2	17.83 $\pm 0.39$	17.82 $\pm 0.39$	17.17 $\pm 0.34$

**Table 8:** A comparison of count rates for different concrete samples with varying carbon content.

The data from Table 7 indicate that the density of the concrete will have a minor impact on the overall results. For this research, each case remained well within  $\pm 2\sigma$  statistical variation. Even though there was no adverse effect from these variations for this research, these simulations prove that the density of the concrete will have an impact on the number of gamma-rays reaching the detectors.

The data from Table 8 shows minor variations in the count rates as the carbon and hydrogen content of the samples widely fluctuated. For each sample, the 50% and 10% cases were within  $\pm 1\sigma$  and  $\pm 2\sigma$ , respectively, of the assumed concentrations. This indicates that an accurate estimate of the carbon and hydrogen content of a concrete sample can be made if the other elemental concentrations of the specimen are well known.

## 4. Conclusions and future work

### 4.1. Conclusions

Several conclusions may be drawn from the research presented in this paper. Primarily, the comparison of the actual and simulated count rates for slab G indicated that a quantitative estimate of the gamma-ray background contribution of concrete is achievable; however, other sources of radiation in the vicinity of the RPM need to be identified and characterized. The comparison of estimated and simulated RPM count rates from slab G indicates that the gamma-ray contribution of a particular concrete can be determined if the environmental background is well known.

The density sensitivity analysis showed that variations at  $\pm 2\sigma$  did not have a significant impact on the average count rate in the RPM detectors. It should be noted that the dimensions and mass of each sample were measured using digital instruments that had a high degree of precision. Low precision instruments will have an adverse impact on the uncertainties in the count rates.

The carbon and hydrogen concentration sensitivity analysis showed that the model is slightly sensitive to large variations in the concentrations of these elements. As long as the sample is well characterized by fast and thermal NAA, it is possible to make a reasonable estimate of the carbon and hydrogen content without the extra time and added costs of additional measurements.

## 4.2. Future work

There are a few areas where this work could be expanded in the future. It was assumed when comparing actual data to the MCNP results, that the RPM was correctly discriminated between 40 and 140 keV. The presence of a slight bias in the MCNP results indicates that this may not be true. If the physical detectors within the RPM employ an energy window larger than what was assumed, the count rate in the RPM would be greater than that predicted by the MCNP model.

In some instances the resources may not be available to conduct a full NAA characterization on a concrete sample. If concretes made with the same aggregate materials have slightly different elemental concentrations, but show comparable gamma-ray attenuation characteristics, it would be possible to use a standardized composition when modeling the material in ISOCS™ and MCNP. This would greatly reduce the time and costs involved in following this method.

Finally, the precision and accuracy of the model could be greatly improved by understanding the environmental background around the RPM. Taking multiple gamma-ray measurements near the RPM over a period of time would provide a data set that could be subtracted from the RPM count rates and provide a more accurate number for comparison with the count rates estimated with MCNP.

## 5. Acknowledgements

The authors would like to thank Dr. William James and Mr. Michael Raulerson of the Texas A&M University CCA for their assistance in carrying out the NAA work described in this paper. The authors would also like to thank the staff at the Texas A&M University NSC for allowing the use of their reactor facility to complete this research.

## 6. References

1. Balatsky, G.I., S.L. Eaton, and W.R. Severe, *Illicit Trafficking of Nuclear and Radiological Materials in Nuclear Safeguards, Security, and Nonproliferation: Achieving Security with Technology and Policy*, edited by J.E. Doyle; Oxford, UK: Butterworth-Heinemann; 2008; pp. 415-433.
2. Ehmann, W.D. and B.F. Ni, *J. Radioanal. Nucl. Chem.*; 160(1); 1992; pp. 169-179.
3. James, W.D., *J. Radioanal. Nucl. Chem.*; 219(2); 1997; pp. 187-190.
4. Bereznaï, T, *Fresenius Z. Anal. Chem.*; 302; 1980; pp. 353-363.
5. MCNP X-5 Monte Carlo Team, "MCNP—A General Purpose Monte Carlo N-Particle Transport Code, Version 5," LA-UR-03 1987, Los Alamos National Laboratory, April 2003, The MCNP5 code can be obtained from the Radiation Safety Information Computational Center (RSICC), P. O. Box 2008. Oak Ridge, TN, 37831-6362.
6. Glascock, M.D., *Tables for Neutron Activation Analysis*; Columbia, MO: University of Missouri Research Reactor Facility; March 1991; pp. 85-86, 101-102.